A model of cytoskeletal reorientation in response to substrate stretching

K. A. Lazopoulos [*]   **A. K. Lazopoulos** [†]
D. Stamenović [‡]

Abstract

Living adherent cells change their orientation in response to substrate stretching such that their cytoskeletal components reorganize in a new direction. To study this phenomenon, we model the cytoskeleton as a planar system of elastic cables and struts both pinned at their endpoints to a flat flexible substrate. Tensed (pre-strained) cables represent actin stress fibers, whereas compression-bearing struts represent microtubules. We assume that in response to uniaxial substrate stretching the model reorients and deforms into a new configuration that minimizes its total potential energy. Using the Maxwell's global stability criterion, we find global minima configurations during static extension and compression of the substrate. Based on these results, we predict reorientation during cyclic stretching of the substrate. We find that in response to cyclic stretching cells either reorient transversely to the direction of stretching, or exhibit multiple configurations symmetrically distributed relative to the direction of stretching. These predictions are consistent with experimental data on living cells from the literature.
Keywords: biomechanics, cytoskeleton, actin, microtubules, total potential, global minimum, stability, substrate stretching, reorientation

1 Introduction

It is well documented in a variety of adherent cell types that cell orientation changes in response to substrate stretching; cells tend to orient either away

---
[*]Mechanics Laboratory, Faculty of Applied Sciences National Technical University of Athens, Athens,Greece

[†]Mechanical Engineering Department, National Technical University of Athens, Athens,Greece

[‡]Department of Biomedical Engineering Boston University, 44 Cummington St., Boston, MA 02215, Massachusetts, USA, e-mail: dimitrij@bu.edu

from the direction of the principle substrate strain [1-10], or parallel with the direction of the principle substrate strain [11-14]. Generally, in response to static or quasi-static substrate extension cells orient parallel with the direction of the principal substrate strain [11,12,14], whereas in response to dynamic (cyclic) substrate stretching, cells align perpendicular to the direction of the principal substrate strain [1-10].

Bischofs and co-workers [15,16] proposed a theoretical model of cell reorientation. A key premise of their model is that the cell favors the orientation entailing the smallest mechanical work invested by the cell's contractile machinery to build up a certain contractile force. Their model predicts that in response to small static substrate extension, the cell always aligns parallel with the direction of extension, whereas in response to substrate compression the cell orients perpendicularly to the direction of compression. It has been also observed that during cell reorientation, its cytoskeleton (CSK) – an intracellular network of filamentous biopolymers – also undergoes reorganization such that cytoskeletal filaments align in the direction consistent with the orientation of the whole cell [5-8,10].

In our previous work, we described cell reorientation as an elastic stability problem [17]. Using the global (Maxwell's) stability criterion, we showed that in response to static uniaxial substrate stretching cells tend to reorient in the direction or away from the direction of the principal substrate strain in order to attain a stable equilibrium configuration, depending whether the elastic properties of the cell are described as a linear Hookean or as a non-convex Mooney-Rivlin material. More recently, Lazopoulos and Pirentis [18] used a similar approach to model reorientation of single actin stress fibers, which are major tension-supporting stress-bearing components of the CSK. Assuming a non-convex strain energy function of stress fibers, they showed that fibers would reorient away from the direction of the principal substrate strain. If, on the other hand, stress fibers were assumed to be linearly elastic, then they would reorient parallel with the direction of applied strain [19].

While all those models have elucidated mechanisms that govern cell reorientation, it is not known how other components of the CSK, most prominently compression-supporting microtubules, contribute to this phenomenon. More importantly, none of the existing models have been used to predict cell reorientation during cyclic substrate stretching. This is important since in their natural habitat many cell types adhere to substrates that undergo cyclic loading (e.g., pulmonary cells during breathing or vascular endothelium during pulsatile blood flow).

Here we propose a microstructural model of the CSK, including both actin stress fibers and microtubules, to study cell reorientation using the stability approach that we used before [17,18]. We first analyze stability of the model

during its reorientation in response to static extension and compression of the substrate. Then we use such obtained results to predict cell orientation during cyclic stretching. We find that predictions are consistent with experimental data on living cells from the literature.

2   Model

To understand basic mechanisms that govern cell reorientation, we propose simple conceptual models of the CSK as follows. We consider two-dimensional planar networks of a rectangular shape (Fig. 1a) and a rhombic shape (Fig. 1b), where the sides (AB, BC, CD, DA) are tensile elements – cables which mimic actin stress fibers, and the diagonals (AC, BD) are compressive elements – struts, which mimic microtubules. The cables and struts are connected to
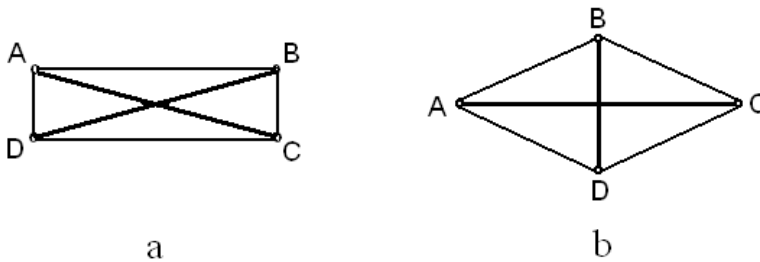

Figure 1: a) Rectangular and b) rhombic models of the cytoskeleton composed of four cables (AB, BC, CD, and DA) and two struts (AC and BD).

the substrate via frictionless pin joints (A, B, C, D); the struts are not joined at their intersection. Interfaces between cables, struts and the substrate are frictionless. We assume that the cables and struts are elastic and that the substrate is flexible (but we do not need to specify its material characteristics). Our key premise is that in response to substrate stretching the CSK assumes a configuration which minimizes its total potential and therefore it is stable. Since steps in the energy minimization procedure for the rectangular and the rhombic model are similar, we give detailed description only for the rectangular model and results for both models.

   Model geometry

   The origin of the $X_1 X_2$ coordinate system is placed at the intersection of the struts (Fig. 2a). The cables are initially tensed such that the initial strain (pre-strain) in the cables is equal. This initial cable tension mimics the presence of pre-existing tensile stress (prestress) in the actin filaments of living cells. The pre-tension in the cables is entirely balanced by the reaction forces at the nodes, implying that the struts are initially unstressed.

The substrate is stretched uniaxially in the direction defined by angle β relative to the X_1-coordinate axis (Fig. 2a). Since data from the literature show that in response to substrate stretching the CSK of living cells reorients and deforms [5-8,10], we assume that in response to substrate stretching our model also reorients and deforms. We view this as a two-step process: first reorientation defined by angle θ relative to the X_1-axis (Fig. 2b) and then stretching-induced deformation superimposed to the rotated configuration (Fig. 2c). Our objective is to show that this new configuration minimizes the potential energy of the model.
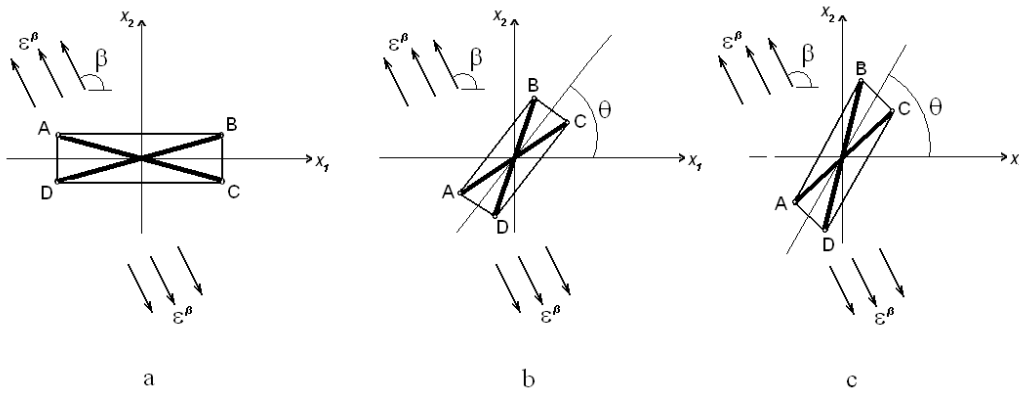

Figure 2: a) The rectangular model of the cytoskeleton is attached to a flexible substrate at the nodes A, B, C and D. The substrate is stretched uniaxially by strain ε^β at angle β elative to the X_1-axis. As a result, the model b) reorients through angle θ relative to the X_1 axis and c) deforms.

2.1 Deformation fields

The initial deformation gradient tensor of a structural component of the model due to pre-strain is $\mathbf{F}_0$. Following substrate stretching, the deformation gradient is

$$\mathbf{F} = \mathbf{F}_\beta \mathbf{F}_\theta \tag{1}$$

where

$$\mathbf{F}_\theta = \mathbf{R}_\theta^T \mathbf{F}_0 \mathbf{R}_\theta \tag{2}$$

is the component of $\mathbf{F}$ due to reorientation through angle θ , with the rotation matrix $\mathbf{R}_\theta$ given as

$$\mathbf{R}_\theta = \begin{bmatrix} \cos\theta & \sin\theta \\ -\sin\theta & \cos\theta \end{bmatrix} \tag{3}$$

relative to the $X_1 X_2$ coordinate system, and

$$\mathbf{F}_\beta = \mathbf{R}_\beta^T \begin{bmatrix} 1 + \varepsilon^\beta & 0 \\ 0 & 1 \end{bmatrix} \mathbf{R}_\beta \qquad (4)$$

is the component of $\mathbf{F}$ due to substrate stretching in the direction defined by angle β, where ε^β is strain (i.e., displacement gradient) of the substrate and $\mathbf{R}_\beta$ is the rotation matrix

$$\mathbf{R}_\beta = \begin{bmatrix} \cos\beta & \sin\beta \\ -\sin\beta & \cos\beta \end{bmatrix} \qquad (5)$$

relative to the $X_1 X_2$ coordinate system.

Let the resting and the pre-strained lengths of cables AB and CD be a_r and a_0, respectively, and of cables BC and DA b_r and b_0, respectively. Assuming that all cables carry the same pre-strain, i.e., same displacement gradient (ε_0), it follows that

$$\varepsilon_0 = \frac{a_0 - a_r}{a_r} = \frac{b_0 - b_r}{b_r} \qquad (6)$$

The corresponding deformation gradient matrices of the cables are

$$\mathbf{F}_0^{AB} = \mathbf{F}_0^{CD} = \begin{bmatrix} 1 + \varepsilon_0 & 0 \\ 0 & 1 \end{bmatrix} \quad \text{and} \quad \mathbf{F}_0^{BC} = \mathbf{F}_0^{DA} = \begin{bmatrix} 1 & 0 \\ 0 & 1 + \varepsilon_0 \end{bmatrix} \qquad (7)$$

The initial deformation gradient for the struts is an identity matrix, $\mathbf{F}_0^{AC} = \mathbf{F}_0^{BD} = \mathbf{I}$, since the struts are assumed initially to be free of strain.

Unit vector $\mathbf{n}$ in the direction of each cable and strut in the rotated configuration (Fig. 2b), defined relative to the $X_1 X_2$ coordinate system, is

$$\mathbf{n} = \begin{bmatrix} \cos\tau \\ \sin\tau \end{bmatrix}, \qquad (8)$$

where $\tau = \theta$ for cables AB and CD, $\tau = \theta + \pi/2$ for cables BC and DA, $\tau = \theta + \phi$ for strut AC and $\tau = \theta - \phi$ for strut BD, where ϕ is defined by,

$$\varphi = \tan^{-1}(a_0/b_0). \qquad (9)$$

The Lagrangean strain e_n of a cable or a strut is

$$e_n = \mathbf{n}^{\mathbf{T}} \mathbf{E} \mathbf{n}, \qquad (10)$$

where

$$\mathbf{E} = \frac{1}{2}(\mathbf{F}^T \mathbf{F} - \mathbf{I}). \qquad (11)$$

On the other hand, e_n is also given as

$$e_n = u_n + \frac{1}{2}u_n^2, \tag{12}$$

where u_n is the displacement gradient of a cable or a strut. We use the non-linear, Lagrangean strain as a metric of deformation of a structural element since in experimental studies the substrate strains are relatively large ($\geq 10\%$) [5-8,10] and thus the Lagrangean strain is more appropriate for describing stretching-induced deformation than the linear strain, which equals u_n. By combining (8)-(12) with (1)-(7), we obtain displacement gradients for cables AB and CD

$$u_{AB} = u_{CD} = -1 + \frac{1}{\sqrt{2}}(1+\varepsilon_0)\sqrt{[2 + 2\varepsilon^\beta + (\varepsilon^\beta)^2 + \varepsilon^\beta(2+\varepsilon^\beta)\cos 2(\beta - \theta)]}, \tag{13}$$

for cables BC and DA

$$u_{BC} = u_{DA} = -1 + \frac{1}{\sqrt{2}}(1+\varepsilon_0)\sqrt{[2 + 2\varepsilon^\beta + (\varepsilon^\beta)^2 - \varepsilon^\beta(2+\varepsilon^\beta)\cos 2(\beta - \theta)]}, \tag{14}$$

for strut AC

$$u_{AC} = -1 + \frac{1}{\sqrt{2}}\sqrt{[2 + 2\varepsilon^\beta + (\varepsilon^\beta)^2 + \varepsilon^\beta(2+\varepsilon^\beta)\cos 2(\beta - \theta - \varphi)]}, \tag{15}$$

and for strut BD

$$u_{BD} = -1 + \frac{1}{\sqrt{2}}\sqrt{[2 + 2\varepsilon^\beta + (\varepsilon^\beta)^2 + \varepsilon^\beta(2+\varepsilon^\beta)\cos 2(\beta - \theta + \varphi)]}. \tag{16}$$

2.2 Stability analysis

The strain energy per unit resting length for each structural member is given as

$$W_n = \frac{1}{2}EAe_n^2, \tag{17}$$

where E is the Young's modulus and A is the cross-section area of a structural member; E is assumed to be equal for the cables and the struts, whereas cross-section area is assumed to be eight times greater for the struts than for the cables. Those assumptions are based on data from the literature [20]. Equation (17) implies a linear relationship between stress and strain e_n, although e_n itself is a nonlinear. This is a generalization of the Hooke's law and is known as a St. Venant-Kirchhoff material. We choose a simple convex strain energy function for structural elements (17) in order to show that it is not necessary

to assume a non-convex strain energy function, as we did previously [17,18], in order to obtain multiple equilibrium configurations. However, a more realistic assumption would be that cables are nonlinearly elastic since they represent actin stress fibers which are known to exhibit a nonlinear behavior [21]. Furthermore, CSK-based microtubules buckle under compression, which is also a non-linear behavior [22].

By substituting (12) into (17), we obtain force (T_n) in each member as follows,

$$T_n = \frac{\partial W_n}{\partial u_n} = EA \left(u_n + \frac{3}{2}u_n^2 + \frac{1}{2}u_n^3 \right). \tag{18}$$

The total potential of the model is defined as

$$V = \sum_{n=1}^{6} (W_n - T_n u_n) l_n, \tag{19}$$

where, l_n is the resting length of a structural member; $n = 1, 2$ correspond to cables AB and CD with the resting length $a_r = a_0/(1 + \varepsilon_0)$ and the cross-sectional area equal to A; $n = 3, 4$ correspond to the cables BC and DA with the resting length equal to $b_r = b_0/(1 + \varepsilon_0)$ and cross-section area equal to A; $n = 5, 6$ correspond to the struts AC and BD with resting length $\sqrt{a_0^2 + b_0^2}$ and cross-section area equal to $8A$. According to (13)-(19), V is a function of cable pre-strain ε_0, substrate strain ε^β, and the difference $\beta - \theta$ between the angles of the direction of stretching and of cell reorientation. Stability demands that at equilibrium V attains minimum, i.e., the following conditions must be satisfied

$$\frac{\partial V}{\partial \theta} = 0 \quad and \quad \frac{\partial^2 V}{\partial \theta^2} > 0. \tag{20}$$

By combining (19) and (20), we can obtain equilibrium values for θ. It is clear from the above formulation that there may exist many equilibrium configurations and that only some of them are stable. We adopt the Maxwell's global stability criterion according to which a configuration of a system is stable if it globally minimizes the total potential [23]. We consider static substrate stretching for the cases when $\varepsilon^\beta > 0$, i.e., the cell is under tension and when $\varepsilon^\beta < 0$, i.e., the cell is under compression. Based on this analysis, we predict cell orientation during of cyclic stretching of the substrate when the cell undergoes periodic tension and compression. In that case, we assume that the stable configuration is the one which yields the smallest difference between the total potentials obtained for tension and compression. This difference may account for energy losses associated with irreversible processes within the cell (see Discussion).

We first assume the following parameter values for the rectangular model: cable reference length $a_0 = 1$; ratio $b_0/a_0 = 0.05$, 0.1, 0.25, 0.50, 0.75 and 1.0 which is indicative of shape; the cross-sectional area of the cables $A = 1$ and of the struts equals 8; the Young modulus of cables and struts $E = 1$; cable pre-strain $\varepsilon_0 = 0.01$, 0.03, 0.05; direction of substrate stretch $\beta = 0.5$, 1.0, and 2.5 rad; and the substrate strain $\varepsilon^\beta = \pm 0.1$ and ± 0.2. In the case of the rhombic model, the shape ratio $b_0/a_0 = 0.05$, 0.1, 0.25, 0.50, 0.75 and 1.0 represents the ratio of the lengths of the diagonal struts (Fig. 1b), whereas the reference (pre-strained) cable length equals $0.5\sqrt{a_0^2 + b_0^2} = 1$. All other parameters have the same meaning and the same values as in the case of the rectangular model. All computations are carried out numerically, using the Mathematica computerized algebra pack.

3   Results

It is found that during extension and compression of the substrate V has multiple global minima which do not depend on the direction of stretching β and pre-strain ε_0 while depend on the shape of the model (i.e., the ratio b_0/a_0) and on the magnitude and the sign of the substrate strain ε^β. Illustrative examples of the stability analysis are given below.

We first consider stability of the rectangular model. For $b_0/a_0 = 0.1$, $\varepsilon_0 = 0.03$, $\beta = 0.5$ rad and $\varepsilon^\beta = \pm 0.1$, during extension (Fig. 3, solid curve), global minima correspond to $\theta = 0.5 \pm 2k\pi$ ($k = 0, 1, 2\ldots$), which is parallel with the direction of ε^β. During compression (Fig. 3, dashed curve), global minima correspond to $\theta = 0.5 \pm (2k + 1)\pi/2$ ($k = 0, 1, 2\ldots$), which is perpendicular to the direction of ε^β. The smallest differences between the total potentials for extension and compression correspond to $\theta = 0.5 \pm (2k + 1)\pi/2$ (Fig. 3), which is perpendicular to the direction of ε^β. Thus, during cyclic stretching the model would orient in the perpendicular direction. Other examples for the rectangular model are given in Table 1 and Figs. 1-7 and for the rhombic model in Table 2 and figs 8-12.

A special case is the situation where $b_0/a_0 = 1$ when the reference shape of both the rectangular and the rhombic models is square. In that case, global minima during extension and compression coincide and are either parallel or perpendicular to the direction of ε^β in the rectangular model (Fig. 7), or at $\pm\pi/4$ relative to the direction perpendicular to the direction of ε^β in the rhombic model (Fig. 12). Thus the smallest differences between the total potentials for extension and compression also correspond to either parallel or perpendicular orientation in the rectangular model (Fig. 7) or to $\pm\pi/4$ relative to the direction perpendicular to the direction of ε^β in the rhombic model (Fig.

12). This, in turn, implies that if $b_0/a_0 = 1$, during cyclic stretching the model would have no preferential orientation. This may be explained by the fact that the since reference shape of the models is square, it cannot create bias for either the parallel or the perpendicular orientation.

Table 1: Predicted values of orientation of the rhombic model following extension, compression and cyclic stretching of the substrate for different sets of parameters b_0/a_0, ε_0, ε^β and β. Orientations are given relative to the direction of stretching (i.e., relative to the direction of ε^β); $\|$ = parallel with the direction of stretching, $\perp$ = perpendicular to the direction of stretching. The last column indicates numbers of the corresponding figures.

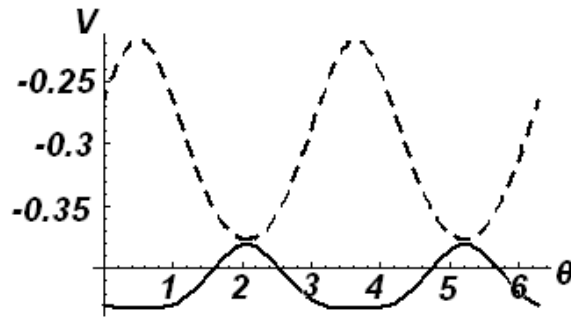| b_0/a_0	ε_0	ε^β	β		*Orientation*			*Fig.#*
			(rad)	*extension*	*compression*	*cyclic*		
0.1	0.03	±0.1	0.5	$\|$	$\perp$	$\perp$		3
0.25	0.05	±0.2	2.5	$\pm\pi/4$	$\perp$	$\perp$		4
0.5	0.01	±0.2	1	$\perp$	$\perp$	$\perp$		5
0.75	0.03	±0.1	0.5	$\|$	$\perp$	$\perp$		6
1	0.03	±0.1	2.5	$\|, \perp$	$\|, \perp$	$\|, \perp$		7

Figure 3: Rectangular model: the total potential (V) vs. angle of orientation (θ) for $b_0/a_0 = 0.1$, $\varepsilon_0 = 0.03$, $\beta = 0.5$ rad, $\varepsilon^\beta = 0.1$ during extension (solid curve), and $\varepsilon^\beta = -0.1$ during compression (dashed curve). Global minima during extension correspond to $\theta = 0.5 \pm 2k\pi$ and during compression to $\theta = 0.5 \pm (2k+1)\pi/2$ ($k = 0, 1, 2\ldots$). The smallest differences between the total potentials for extension and compression correspond to $\theta = 0.5\pm(2k+1)\pi$.
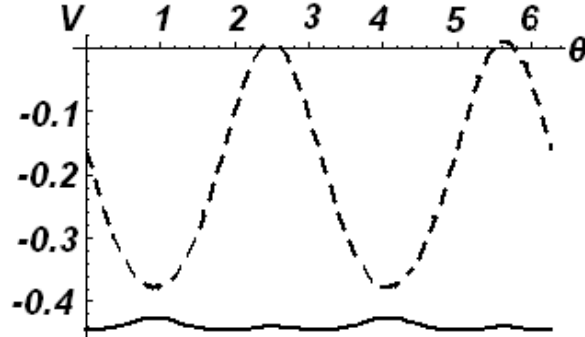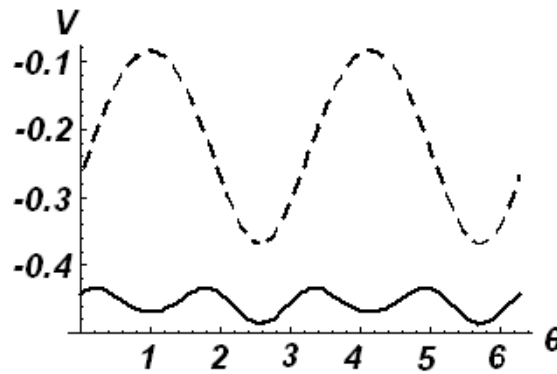
Figure 4: Rectangular model: the total potential energy (V) vs. angle of orientation (θ) for $b_0/a_0 = 0.25$, $\varepsilon_0 = 0.05$, $\beta = 2.5$ rad, $\varepsilon^\beta = 0.2$ during extension (solid curve), and $\varepsilon^\beta = -0.2$ during compression (dashed curve). Global minima during extension correspond to $\theta = (2.5 \pm k\pi) \pm \pi/4$ and during compression to $\theta = 2.5 \pm (2k + 1)\pi/2$ $(k = 0,1,2\ldots)$. The smallest differences between the total potentials for extension and compression correspond to $\theta = 2.5 \pm (2k + 1)\pi/2$.

Figure 5: Rectangular model: the total potential (V) vs. angle of orientation (θ) for $b_0/a_0 = 0.5$, $\varepsilon_0 = 0.01$, $\beta = 1$ rad, $\varepsilon^\beta = 0.2$ during extension (solid curve), and $\varepsilon^\beta = -0.2$ during compression (dashed curve). Global minima during extension and compression correspond to $\theta = 1 \pm (2k + 1)\pi/2$ $(k = 0,1,2\ldots)$. The smallest differences between the total potentials for extension and compression correspond to $\theta = 1 \pm (2k + 1)\pi/2$.
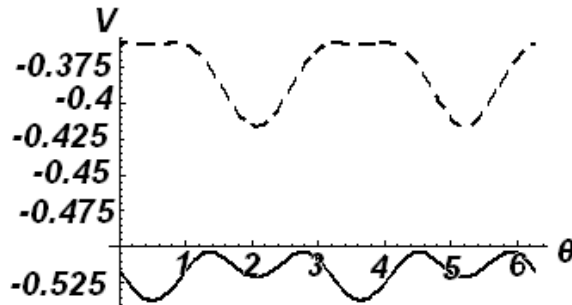
Figure 6: Rectangular model: the total potential energy (V) vs. angle of orientation (θ) for $b_0/a_0 = 0.75$, $\varepsilon_0 = 0.03$, $\beta = 0.5$ rad, $\varepsilon^\beta = 0.1$ during extension (solid curve), and $\varepsilon^\beta = -0.1$ during compression (dashed curve). Global minima during extension correspond to $\theta = 0.5 \pm k\pi$ and during compression to $\theta = 0.5 \pm (2k+1)\pi/2$ ($k = 0, 1, 2\ldots$). The smallest differences between the total potentials for extension and compression correspond to $\theta = 0.5 \pm (2k+1)\pi/2$.
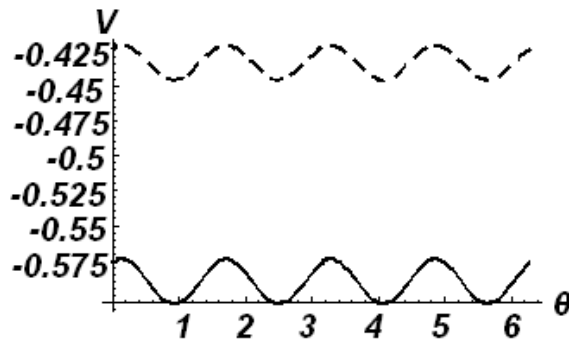

Figure 7: Rectangular model: the total potential (V) vs. angle of orientation (θ) for $b_0/a_0 = 1$, $\varepsilon_0 = 0.03$, $\beta = 2.5$ rad, $\varepsilon^\beta = 0.1$ during extension (solid curve), and $\varepsilon^\beta = -0.1$ during compression (dashed curve). Global minima during extension and compression correspond to $\theta = 2.5 \pm k\pi/2$ ($k = 0,1,2\ldots$). The smallest differences between the total potentials for extension and compression correspond to $\theta = 2.5 \pm k\pi/2$.

Table 2: Predicted values of orientation of the rectangular model following extension, compression and cyclic stretching of the substrate for different sets of parameters b_0/a_0, ε_0, ε^β and β. Orientations are given relative to the direction of stretching (i.e., relative to the direction of ε^β); $\|$ = parallel with the direction of stretching, $\perp$ = perpendicular to the direction of stretching. The last column indicates numbers of the corresponding figures.

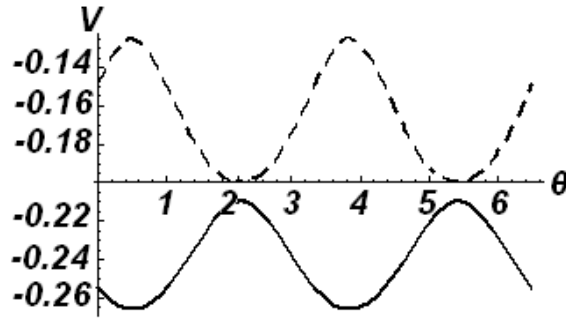| b_0/a_0	ε_0	ε^β	β		*Orientation*		*Fig.#*
			(rad)	*extens.*	*compression*	*cyclic*	
0.1	0.03	± 0.1	0.5	$\|$	$\perp$	$\perp$	8
0.25	0.05	± 0.2	2.5	$\|$	$\perp$	$\perp$	9
0.5	0.01	± 0.2	1	± 0.65	$\pm 0.65 + \pi/2$	$\pm 0.65 + \pi/2$	10
0.75	0.03	± 0.1	0.5	± 0.65	$\pm 0.65 + \pi/2$	$\pm 0.65 + \pi/2$	11
1	0.03	± 0.1	2.5	$\pm\pi//4$	$\pm\pi//4$	$\pm\pi//4$	12

Figure 8: Rhombic model: the total potential (V) vs. angle of orientation (θ) for $b_0/a_0 = 0.1$, $\varepsilon_0 = 0.03$, $\beta = 0.5$ rad, $\varepsilon^\beta = 0.1$ during extension (solid curve), and $\varepsilon^\beta = -0.1$ during compression (dashed curve). Global minima during extension correspond to $\theta = 0.5 \pm 2k\pi$ and during compression to $\theta = 0.5 \pm (2k+1)\pi/2$ ($k = 0,1,2\ldots$). The smallest differences between the total potentials for extension and compression correspond to $\theta = 0.5 \pm (2k+1)\pi$.
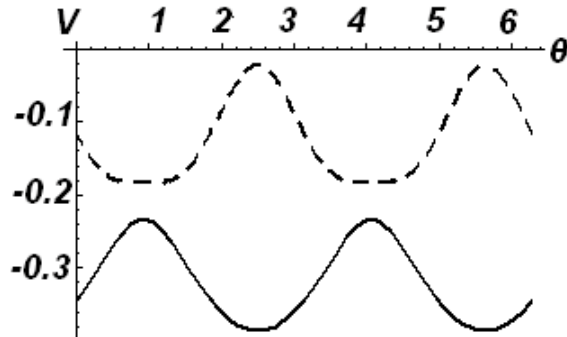
Figure 9: Rhombic model: the total potential (V) vs. angle of orientation (θ) for $b_0/a_0 = 0.25$, $\varepsilon_0 = 0.05$, $\beta = 2.5$ rad, $\varepsilon^\beta = 0.2$ during extension (solid curve), and $\varepsilon^\beta = -0.2$ during compression (dashed curve). Global minima during extension correspond to $\theta = 2.5 \pm 2k\pi$ and during compression to $\theta = 2.5 \pm (2k + 1)\pi/2$ ($k = 0,1,2\ldots$). The smallest differences between the total potentials for extension and compression correspond to $\theta = 2.5 \pm (2k + 1)\pi$.
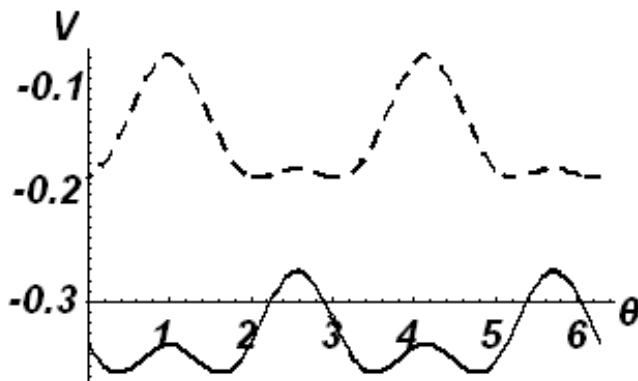

Figure 10: Rhombic model: the total potential (V) vs. angle of orientation (θ) for $b_0/a_0 = 0.5$, $\varepsilon_0 = 0.01$, $\beta = 1$ rad, $\varepsilon^\beta = 0.2$ during extension (solid curve), and $\varepsilon^\beta = -0.2$ during compression (dashed curve). Global minima during extension correspond to $\theta = (1 \pm k\pi) \pm 0.65$ and during compression to $\theta = [1 \pm (2k + 1)\pi/2] \pm 0.65$ ($k = 0,1,2\ldots$). The smallest differences between the total potentials for extension and compression correspond to $\theta = [1 \pm (2k + 1)\pi/2] \pm 0.65$.

Figure 11: Rhombic model: the total potential (V) vs. angle of orientation (θ) for $b_0/a_0 = 0.75$, $\varepsilon_0 = 0.03$, $\beta = 0.5$ rad, $\varepsilon^\beta = 0.1$ during extension (solid curve), and $\varepsilon^\beta = -0.1$ during compression (dashed curve). Global minima during extension correspond to $\theta = (0.5 \pm k\pi) \pm 0.65$ and during compression to $\theta = [0.5 \pm (2k + 1)\pi/2] \pm 0.65$ ($k = 0,1,2\ldots$). The smallest differences between the total potentials for extension and compression correspond to $\theta = [0.5 \pm (2k + 1)\pi/2] \pm 0.65$.
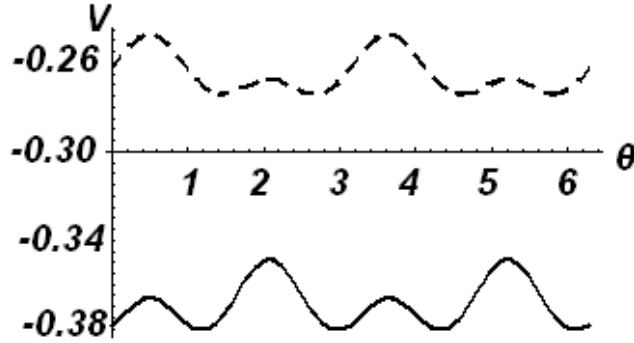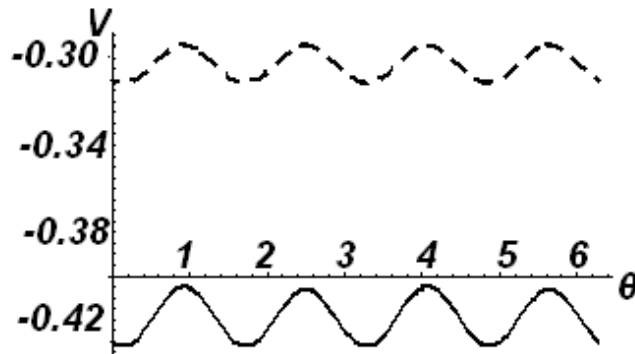
Figure 12: Rhombic model: the total potential (V) vs. angle of orientation (θ) for $b_0/a_0 = 1$, $\varepsilon_0 = 0.03$, $\beta = 2.5$ rad, $\varepsilon^\beta = 0.1$ during extension (solid curve), and $\varepsilon^\beta = -0.1$ during compression (dashed curve). Global minima during extension and compression correspond to $\theta = 2.5 \pm (2k+ 1)\pi/4$ ($k = 0,1,2\ldots$).. The smallest differences between the total potentials for extension and compression correspond to $\theta = 2.5 \pm (2k+ 1)\pi/4$.

4   Discussion

The most significant results of this study is that simple microstructural models of the CSK can predict cell orientation in response to static and cyclic stretching that are consistent with experimental data from the literature; namely that during static extension cells align in the direction parallel with the direction of stretching and that during cyclic stretching they align perpendicular to the direction of stretching [1-14]. The analysis also shows that for certain set of parameter values multiple equilibrium configurations are possible. This is also consistent with previously reported experimental data [5].

The results of the stability analysis are dependent on the shape of the model. In the case of the rhombic model, more elongated shapes (i.e., smaller ratio b_0/a_0), are stable when aligned parallel with the direction of stretching during extension and perpendicular to the direction of stretching during compression and during cyclic loading. In the case of the rectangular model, there is no such systematic dependence of cell orientation on the b_0/a_0 ratio. Our analysis also shows that reorientation depends on the magnitude of the substrate strain, but there is no systematic dependence. This differs from experimental studies which show that the greater the substrate strain, the closer the cell alignment with the perpendicular direction during cyclic stretching [3,5]. A possible explanation for this discrepancy could be the assumption that the cables and struts are linearly elastic. In our previous non-linearly elastic models, we obtained a dependence on substrate strain that is consistent with experimental observations [17,18].

Stability analysis shows that global minima do not depend on the direction β of stretching and on the pre-strain ε_0 in the cable elements. The former is consistent with experimental data which show that initially randomly oriented cells eventually reorient in the same direction following stretching [1-14]. The latter is not consistent with experiments which show that a decrease in pre-stress in actin filaments, and presumably a decrease in pre-strain, leads to a closer alignment with the direction of stretching [6,8]. Again, this discrepancy may reflect the material linearity assumption for cables and struts; in our previous nonlinear models we obtained that orientation depends on the pre-strain in a manner consistent with the experiments [17,18].

Predictions of reorientation during cyclic stretching are based on the assumption that the stable configurations are those for which the differences in the total potential between tension and compression are the smallest. In living cells, this difference may account for the energy losses per stretching cycle due to irreversible processes within cells (e.g., cytoskeletal viscoelasticity, remodeling, etc.) [24,25]. However, energy losses reduce cell's functional efficiency, and therefore the cell would tend to attain configurations which minimize those

loses.

Our choice of the simple quadratic strain energy function for structural elements (17) shows that it is not necessary to invoke a non-convex strain energy function in order to obtain multiple equilibrium configurations [17,18]. On the other hand, experimental data [21] suggest that a non-quadratic convex strain energy function for actin stress fibers is more realistic (e.g., adding a quartic term strain in equation (17)). We believe that such an equation would only make calculations more complex while not providing a deeper physical insight. Moreover, for strains that do not exceed $\sim 40\%$, the stress-strain behavior of the stress fibers is linear [21], whereas in our examples we considered strains that do not exceed 5% (see Tables 1 and 2). Thus, our assumption of the quadratic strain energy function is justified.

We do not consider in our model the possibility that microtubules may buckle under compression. However, buckling of microtubules does occur in cells. Incorporating this buckling into our model would certainly provide a more realistic depiction of the cellular events [22], while increasing the model's complexity at the expense of its mathematical transparency. Considering that the model is capable of describing cell reorientation that is consistent with experimental data, we believe that inclusion of buckling of microtubules into the model is not essential.

We do not consider the contribution of material properties of the substrate to stability. Bischofs and colleagues [15,16] showed that cell tend to orient in the direction higher effective substrate stiffness. This, in turn, suggests that including the contribution of substrate elasticity into our model may further bias its reorientation.

From a biological point of view, this study can provide a framework for better understanding of physiological functions of adherent cells. For example, pulmonary airways *in vivo* undergo non-uniform cyclic stretching [26], which is the likely cause that sets the orientation of smooth muscle cells around the airway. Smooth muscle orientation is a very important determinant of airway responsiveness in health and disease [27,28]. Second, healthy vascular endothelial cells change their orientation in response to stretching of the blood vessel. While this reorientation is linked to a coupling between mechanical signals from the environment and biochemical signals within the cell [8], it is not clear how mechanical signals from the environment and mechanical signals within the cell cooperate and drive the cell to a new orientation.

In summary, the stability analysis of the simple models of the CSK can predict reorientation of cells during both static and cyclic stretching of the substrate that is consistent with experimental data from the literature. While these models represent an overly simplified and crude representation of the CSK, the good agreements between model predictions and experimental data

from the literature suggest that the proposed approach can provide a useful framework for more complex studies of mechanical interactions between cell and the substrate.

References

[1] P. C. Dartsch and H. Hämmerle, Orientation response of arterial smooth muscle cells to mechanical stimulation, Eur. J. Cell. Biol., 41, (1986), 339–346.

[2] T. Iba and B. E. Sumpio, B. E., Morphological response of human endothelial cells subjected to cyclic strain *in vitro*, Microvasc. Res., 42, (1991), 245-254.

[3] C. Neidlinger-Wilke, E. S. Grood, J. H.-C., Wang, R. A. Brand and L. Claes, Cell alignment is induced by cyclic changes in cell length: studies of cells grown in cyclically stretched substrates, J. Orthop. Res., 19, (2001), 286-293.

[4] P. Sipkema, J. W. van der Linden, N. Westerhof and F. C.-P. Yin, Effect of cyclic axial stretch of rat arteries on endothelial cytoskeletal morphology and vascular reactivity, J. Biomech., 36, (2003), 653-659.

[5] T. Takemasa, K. Sugimoto and K. Yamashita, Amplitude-dependent stress fiber reorientation in early response to cyclic strain, Exp. Cell Res., 230, (1997), 407-410.

[6] J. H.-C. Wang, P. Goldschmidt-Clermont and F. C.-P. Yin, Contractility affects stress fiber remodeling and reorientation of endothelial cells subjected to cyclic mechanical stretching, Ann. Biomed. Eng., 28, (2000), 1165-1171.

[7] J. J. Wille, C. A. Ambrosi and F. C.-P. Yin, Comparison of the effects of cyclic stretching and compression on endothelial cell morphological responses, ASME J. Biomech. Eng., 126, (2004), 545-551.

[8] R. Kaunas, P. Nguyen, S. Usami and S. Chien, Cooperative effects of Rho and mechanical stretch on stress fiber organization, Proc. Natl. Acad. Sci. USA, 102, (2005),15895-15900.

[9] K. Kurpinski, J. Chu, C. Hashi and S. Li, Anisotropic mechanosensing by mesenchimal stem cells, Proc. Natl. Acad. Sci. USA, 103, (2006), 16095-16100.

[10] J. H.-C. Wang, P. Goldschmidt-Clermont, J. Wille, J. and F. C.-P.Yin, Specificity of endothelial cell reorientation in response to cyclic mechanical stretching, J. Biomech., 34, (2001), 1563-1572.

[11] M. Eastwood,V. C. Mudera,D. A. McgroutherR. A. and Brown, Effect of precise mechanical loading on fibroblast populated collagen lattices: Morphological changes, Cell Motil. Cytoskeleton, 40, (1998), 13-21.

[12] A. Ignatius, H. Blessing, A. Liedert, D. Kaspar, L. Kreja, B. Friemert, and L. Claes, Effects of mechanical strain on human osteoblastic precursor cells in type I collagen matrices, Orthopade, 33, (2004), 1386-1393.

[13] A. M. Collinsworth, C. E. Torgan, S. N. Nagada, R. J. Rajalingam, W. E. Kraus and G. A. Truskey, G. A., Orientation and length of mammalian skeletal myocytes in response to unidirectional stretch, Cell Tissue Res., 302, (2000) 243-251.

[14] K. Takakuda and H. Miyairi, Tensile behavior of fibroblasts cultured in collagen gel, Biomaterials, 17, (1996), 1393-1397.

[15] I. B. Bischofs, S. A. Safran and U. S. Schwarz, Elastic interactions of active cells with soft materials, Phys. Rev. E, 69, (2004), 021911.

[16] I. B. Bischofs and U. S. Schwarz, U. S., Cell organization in soft media due to active mechanosensing, Proc. Natl. Acad. Sci. USA, 100, (2003) 9274-9279.

[17] K. A. Lazopoulos and D. Stamenović, A mathematical model of cell reorientation in response to substrate stretching, Mol. Cell. Biomech., 3, (2006), 43-48.

[18] K. A. Lazopoulos and A. Pirentis, Substrate stretching and reorganization of stress fibers as a finite elasticity problem. Int. J. Solids Struct., 44, (2007), 8285-8296.

[19] J. H.-C. Wang, Substrate deformation determines actin cytoskeleton reorganization: mathematical modeling and experimental study, J. Theor. Biol., 202, (2000), 33-41.

[20] F. Gittes, B. Mickey, J. Nettleton and J. Howard, J., Flexural rigidity of microtubules and actin filaments measured from thermal fluctuations in shape, J. Cell Biol., 120, (1993), 923-934.

[21] S. Deguchi, S. Ohashi and M. Sato, Tensile properties of single stress fibers isolated from cultured vascular smooth muscle cells, J. Biomech. 39, (2006), 2603-2610.

[22] D. Stamenović, S. M. Mijailovich, I. M. Toli-Nørrelykke, J. Chen and N. Wang, Cell prestress. II. Contribution of microtubules, Am. J. Physiol. Cell Physiol., 282, (2002), C617-C624.

[23] J. L. Ericksen, Introduction to the Thermodynamics of Solids, ed. R. J. Knops and K. W. Morton, Chapman & Hall, London, UK, chap. 3, (1991), 39-61.

[24] B. Fabry, G. N. Maksym, J .P. Butler, M. Glogauer, D. Navajas and J. J Fredberg, Scaling the microrheology of living cells, Phys. Rev. Lett., 87, (2001), 148102.

[25] N. Rosenblatt,S. Hu, J. Chen, N. Wang and D. Stamenović, Distending stress of the cytoskeleton is a key determinant of cell rheological behaviour, Biochem. Biophys. Res. Commun., (2004), 321, 617-622.

[26] R. H. Brown and W. Mitzner, Effect of lung inflation and airway muscle tone on airway diameter in vivo, J. Appl. Physiol., 80, (1996), 1581-1588.

[27] J. H. Bates and J. G. Martin, A theoretical study of the effect of airway smooth muscle orientation on bronchoconstriction, J. Appl. Physiol., 69, (1990), 995-1001.

[28] S. M. Smiley-Jewell, M. U. Tran, A. J. Weir, Z. A. Johnson, L. S. Van Winkle and C. G. Plopper, Three-dimensional mapping of smooth muscle in the distal conducting airways of mouse, rabbit, and monkey, J. Appl. Physiol., 93, (2002), 1506-1514.

Model reorijentacije citoskeleta usled mehaničkog istezanja substrata ćelije

Žive ćelije menjaju svoju orijentaciju usled mehaničkog istezanja substrata za koji ćelije prianjaju, pri čemu se komponente ćelijskog citoskeleta reorganizuju u pravcu nove orijentacije. U ovom radu razmatrali smo ovaj fenomen modelirajući citoskelet kao planarni sistem elastičnih užadi i štapova koji su na svojim krajevima prikačeni za elastični substrat. Užad su zategnuta i predstavljaju aktinska vlakna, dok štapovi nose pritisne sile i predstavljaju mikrotubule. Naša radna pretpostavka je da se usled istezanja substrata model deformiše i menja svoju početnu orijentaciju tako što zauzima novu konfiguraciju koja minimizira njegovu totalnu potencijalnu energiju. Koristeći Maksvelov globalni kriterijum elastične stabilnosti, izračunali smo globalne minimume potencijalne energije modela za slučajeve jednoosnog istezanja i kompresije substrata. Koristeći ove rezultate, predvideli smo ćelijsku reorijentaciju u uslovima cikličnog istezanja-kompresije substrata. Dobili smo da se u ovom slučaju ćelije orijentišu ili upravno na pravac glavne deformacije, ili da zauzimaju višestruke konfiguracije simetrično rasporedjene u odnosu na pravac glavne deformacije. Ova predvidjanja su saglasna sa eksperimentalnim podacima iz literature.